J Mater Sci (2016) 51:5321–5329

Effects of alloying elements on crystallization kinetics of Ti–Zr–Be bulk metallic glass

Pan Gong[1,2,*], Xin Wang[3], and Kefu Yao[2]

[1] State Key Laboratory of Materials Processing and Die & Mould Technology, Huazhong University of Science and Technology, 1037 Luoyu Road, Wuhan 430074, Hubei, China
[2] School of Materials Science and Engineering, Tsinghua University, Beijing 100084, China
[3] School of Materials Science and Engineering, Hebei University of Technology, Tianjin 300130, China

Received: 10 November 2015
Accepted: 13 February 2016
Published online: 22 February 2016

ABSTRACT

It has been found that the partial substitution of Fe, Al, Ag, Cu, Ni, V, or Cr for Be effectively enhances the glass-forming ability of Ti–Zr–Be ternary alloy. The influence of different alloying elements on crystallization kinetics of $Ti_{41}Zr_{25}Be_{34}$ alloy has been investigated by isothermal and isochronal differential calorimetry combined with X-ray diffraction. Among the selected alloying elements, Fe, Al, Cu, Ni, or Cr can enhance the thermal stability, while the Ag- and V-containing alloys exhibit a slightly narrower supercool liquid region. The crystallization of all the eight alloys proceeds through at least two exothermic events. The apparent activation energies of glass transition and crystallization have been determined based on the Kissinger equation. The substitution of Al, Ag, Cu, or Ni for Be does not change the product of the primary crystallization of the base alloy. However, with the addition of beta stabilized elements (Fe, V, and Cr), the formation of β-Ti as primary phase is promoted. The overall nucleation and growth characteristics of the parent, Al-, Ag-, Cu-, Ni-, V-, and Cr-additive alloys, are similar. Compared with the other seven alloys, $Ti_{41}Zr_{25}Be_{28}Fe_6$ alloy exhibits much larger Avrami exponents with an average value of 5.26, indicating a high-dimensional growth with increasing nucleation rate.

Introduction

Lightweight bulk metallic glasses (BMGs), which are represented by Al- [1, 2], Mg- [3, 4], and Ti-based BMGs [5–8], have attracted much attention due to the modern concepts for lightweight construction. However, the glass-forming ability (GFA) of Al-based BMGs is very poor while most of Mg-based BMGs are very brittle. In this sense, Ti-based BMGs seem more promising materials to be used in industry fields such as aerospace. In the past decades, a series of Ti-based BMGs, such as Ti–Cu–Ni [9], Ti–Zr–Cu–Ni–Sn [10], Ti–Zr–Cu–Ni–Be [11], Ti–Zr–Cu–Pd–Sn [12], and Ti–Zr–Hf–Cu–Ni–Si–Sn [13], have been successfully developed. However, in order to improve the GFA,

Address correspondence to E-mail: gongpan126@126.com

DOI 10.1007/s10853-016-9835-5

most of the available Ti-based BMGs always contain a large portion of heavy elements (e.g., Cu, Pd, etc.), resulting in the decrease of specific strength.

Compared with other developed Ti-based BMGs, Ti–Zr–Be ternary alloys [14, 15] possess relatively high specific strength because of the addition of light element Be. However, the critical size for glass formation of Ti–Zr–Be alloys is no more than 6 mm [15], which is relatively small compared with that of some well-known ternary BMGs (e.g., Zr–Ni–Al [16], Mg–Cu–Y [17], etc.). In order to solve this problem, alloying method, which is widely used to improve the properties of alloys, has been adopted to enhance the GFA of $Ti_{41}Zr_{25}Be_{34}$ alloy. In previous work, it has been found that the GFA of $Ti_{41}Zr_{25}Be_{34}$ BMG can be greatly improved by replacing Be by Al [18] or some transitional elements (e.g., Fe [19], Ag [20], Cu [21], Ni [22], V [14], and Cr [15]). Moreover, the optimized alloying content for most of the selected elements is around 6 at.%. Unfortunately, the underlying mechanisms of GFA improvement of $Ti_{41}Zr_{25}Be_{34}$ alloy induced by alloying have not been fully understood yet.

As the glass formation is a competing process between liquid phase and competing crystalline phases, research on the crystallization kinetics of is helpful to further understand the GFA [23–25]. In this study, the crystallization behaviors of $Ti_{41}Zr_{25}Be_{34}$ and seven representative quaternary BMGs with different fourth elements have been investigated by X-ray diffraction (XRD) and differential scanning calorimetry (DSC) under both isochronal and isothermal conditions. Based on the experimental results, the roles of alloying elements on crystallization kinetics of $Ti_{41}Zr_{25}Be_{34}$ alloy have been exposed.

Experimental procedure

Master ingots with nominal compositions of $Ti_{41}Zr_{25}Be_{34}$ and $Ti_{41}Zr_{25}Be_{28}M_6$ (M = Fe, Al, Ag, Cu, Ni, V, and Cr) were prepared by arc melting high purity (>99.9 wt%) constituent elements under a Ti-gettered argon atmosphere. From the ingots, cylindrical alloy rods with different diameters were prepared by copper mold casting method. The amorphous nature of as-cast samples was ascertained by X-ray diffraction (XRD, Rigaku D/max-RB) with Cu Kα radiation. Thermal analysis was carried out in a differential scanning calorimeter (DSC, NETZSCH 404 F1 Pegasus). The DSC system was calibrated for temperature and enthalpy using indium and zinc standards. Continuous heating was carried out at different heating and cooling rates (5, 10, 20, and 40 K min^{-1}) with a flow of purified argon gas using a platinum pan with alumina liner. In the case of isothermal annealing, the samples were put in aluminum pan and heated to the selected temperature at a heating rate of 150 K min^{-1}, and then held until the crystallization completed. In order to eliminate the sample size effect, the DSC samples were cut from ϕ 3 mm as-cast rods and the weight of each sample was between 10 and 20 mg. In order to find out the crystalline phases corresponding to different crystallization steps, 3 mm diameter samples were heated to the selected temperatures in DSC at a heating rate of 20 K min^{-1}. After cooling, the annealed samples were polished to remove the oxide layer on the surface and examined by XRD.

Results and discussion

Figure 1 shows the XRD patterns of $Ti_{41}Zr_{25}Be_{34}$ and $Ti_{41}Zr_{25}Be_{28}M_6$ (M = Fe, Al, Ag, Cu, Ni, V, and Cr) rods with their critical diameters (D_c). All the patterns consist of only a broad diffraction halo peak without any sharp Bragg peak, indicating the amorphous structure of the as-cast rods. The critical diameter of ternary $Ti_{41}Zr_{25}Be_{34}$ alloy (base alloy) is only 5 mm. However, with the addition of different fourth elements, the glass-forming ability can be improved in varying degrees. Among all the seven selected elements, Cu and Ni are the best choices for improving the GFA as $Ti_{41}Zr_{25}Be_{28}Cu_6$ and $Ti_{41}Zr_{25}Be_{28}Cu_6$ alloys possess a relatively large critical diameter of 15 mm, which is three times as that of the base alloy. Even for the worst element V, the critical size can also be enhanced from 5 to 6 mm. The above results confirm that alloying method is really effective to enhance the GFA of Ti–Zr–Be ternary alloy.

Figures 2 and S1 show the continuous heating DSC curves of $Ti_{41}Zr_{25}Be_{34}$ and $Ti_{41}Zr_{25}Be_{28}M_6$ (M = Fe, Al, Ag, Cu, Ni, V, and Cr) glassy alloys measured at the heating rates of 5, 10, 20, and 40 K min^{-1}. The characteristic temperatures such as T_g (the glass transition temperature), T_x (the onset temperature of crystallization), and T_{p1} (the first crystallization peak temperature) are marked on the DSC curves and their values are listed in Table 1. It is worthwhile to note

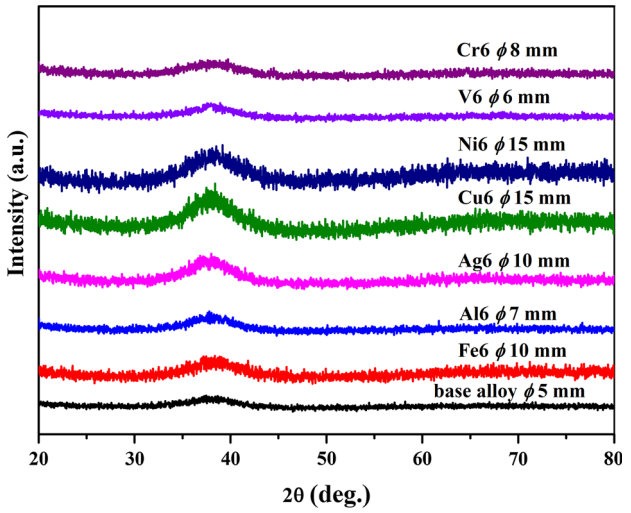

Figure 1 XRD patterns of $Ti_{41}Zr_{25}Be_{34}$ and $Ti_{41}Zr_{25}Be_{28}M_6$ (M = Fe, Al, Ag, Cu, Ni, V, and Cr) as-cast rods with their critical diameters.

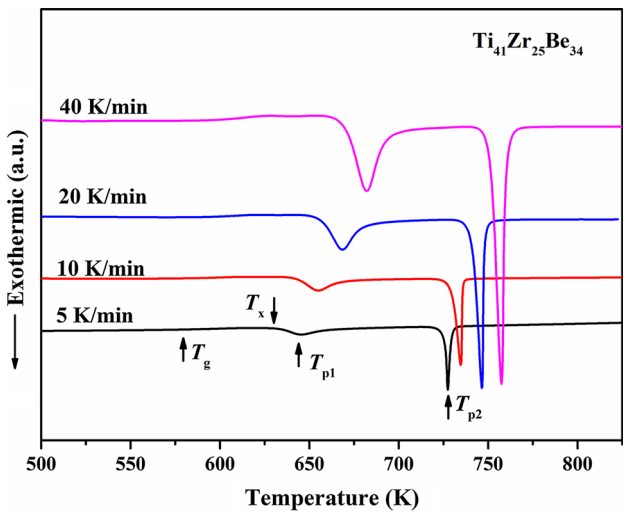

Figure 2 Isochronal DSC curves of $Ti_{41}Zr_{25}Be_{34}$ alloy at different heating rates.

that the crystallization behavior can be changed by the addition of some alloying elements. As shown in Fig. 2, the base alloy has a two-stage crystallization with a relatively sharp second exothermic event. With the addition of Al, Ag, Cu, V, or Cr, the corresponding quaternary alloys exhibit similar crystallization behavior. In turn, the Fe bearing alloy has a two-stage crystallization with a relatively sharp first peak and the Ni containing alloy shows three-stage crystallization. It can also be found that the supercooled liquid region (defined as $\Delta T_x = T_x - T_g$) increases with the addition of Fe, Al, Cu, Ni, or Cr. Among all the alloys listed in Table 1, $Ti_{41}Zr_{25}Be_{28}Fe_6$ alloy possesses the widest supercooled liquid region of over 100 K, which is larger than that of most developed Ti-based BMGs. However, the GFA of $Ti_{41}Zr_{25}Be_{28}Fe_6$ alloy is not as good as $Ti_{41}Zr_{25}Be_{28}Cu_6$ and $Ti_{41}Zr_{25}Be_{28}Ni_6$ alloys which possess a smaller ΔT_x value. Moreover, ΔT_x decreases slightly with Ag or V addition but the GFA has been improved. In this sense, although ΔT_x is always used as an indicator of the GFA for BMGs, the relationship between ΔT_x and GFA of Ti–Zr–Be–M glassy alloys seems weak. Similar phenomena have been reported in some other alloy systems [26].

From Figs. 2, S1 and Table 1, it can also be seen that the characteristic temperatures of all the listed alloys are shifted to higher temperature side with increasing heating rates. The activation energy of the glass transition or crystallization reaction under continuous heating condition can be calculated by the Kissinger equation [27]:

$$\ln\left[\frac{\beta}{T^2}\right] = -\frac{E}{\mathrm{RT}} + C, \quad (1)$$

where β is the heating rate, E is the apparent activation energy for the process, R is the gas constant, T represents the characteristic temperature (such as T_g, T_x, and T_{p1}), and C is a constant. Figure 3 shows the Kissinger plots of glassy alloys calculated by T_g, T_x and T_{p1}, respectively. The calculated activation energy of the glass transition and crystallization are listed in Table 1. For all the eight alloys, E_g is higher than E_x and E_{p1}, indicating that the glass transition needs more activation energy than the crystallization reaction. It has been presumed that E_x and E_{p1} represent the activation energy for nucleation and growth, respectively [28]. As shown in Table 1, E_{p1} of $Ti_{41}Zr_{25}Be_{28}Ag_6$ alloy is slightly higher than E_x, which means the growth process of the crystalline phases is more difficult than the nucleation process. Correspondingly, the other seven alloys are just the reverse. From Table 1, we can also find that E_g, E_x, and E_{p1} of the present alloy series have no obvious relationship with ΔT_x and GFA. Among all the listed eight alloys, $Ti_{41}Zr_{25}Be_{28}V_6$ alloy has the largest E_g, while $Ti_{41}Zr_{25}Be_{28}Ag_6$ alloy has the largest E_x and E_{p1}. However, the critical diameter D_c and ΔT_x of these two alloys are not the largest according to the experimental results provided in Fig. 1 and Table 1. It has been reported that Ag addition enhances the glass-forming ability and enlarge the supercooled

Table 1 Thermal data, activation energy, and glass-forming ability of $Ti_{41}Zr_{25}Be_{34}$ and $Ti_{41}Zr_{25}Be_{28}M_6$ (M = Fe, Al, Ag, Cu, Ni, V, and Cr) bulk metallic glasses

Alloys	Heating rate (K min^{-1})	T_g (K)	T_x (K)	T_{p1} (K)	ΔT_x (K)	E_g (kJ mol^{-1})	E_x (kJ mol^{-1})	E_{p1} (kJ mol^{-1})	D_c (mm)
$Ti_{41}Zr_{25}Be_{34}$	5	578.6 ± 3.0	631.0 ± 1.0	643.0 ± 1.0	52.4	273.9 ± 12.5	175.7 ± 2.2	181.3 ± 2.4	5
	10	584.8 ± 3.0	643.0 ± 1.0	655.1 ± 1.0	58.2				
	20	591.4 ± 3.0	656.3 ± 1.0	668.9 ± 1.0	64.9				
	40	599.8 ± 3.0	670.1 ± 1.0	682.2 ± 1.0	70.3				
$Ti_{41}Zr_{25}Be_{28}Fe_6$	5	586.5 ± 3.0	692.8 ± 1.0	699.5 ± 1.0	106.3	264.5 ± 8.4	171.2 ± 9.5	179.4 ± 6.3	10
	10	593.7 ± 3.0	705.9 ± 1.0	712.4 ± 1.0	112.2				
	20	600.3 ± 3.0	723.0 ± 1.0	727.1 ± 1.0	122.7				
	40	609.3 ± 3.0	740.8 ± 1.0	746.8 ± 1.0	131.5				
$Ti_{41}Zr_{25}Be_{28}Al_6$	5	600.5 ± 3.0	670.7 ± 1.0	684.0 ± 1.0	70.2	244.9 ± 21.4	201.5 ± 9.3	222.5 ± 6.8	7
	10	609.2 ± 3.0	683.1 ± 1.0	694.8 ± 1.0	73.9				
	20	615.0 ± 3.0	694.1 ± 1.0	706.6 ± 1.0	79.1				
	40	626.5 ± 3.0	709.8 ± 1.0	720.4 ± 1.0	83.3				
$Ti_{41}Zr_{25}Be_{28}Ag_6$	5	580.5 ± 3.0	640.6 ± 1.0	647.6 ± 1.0	60.1	259.7 ± 17.9	256.8 ± 16.9	242.5 ± 21.9	10
	10	587.8 ± 3.0	647.5 ± 1.0	654.4 ± 1.0	59.7				
	20	593.6 ± 3.0	656.9 ± 1.0	664.3 ± 1.0	63.3				
	40	603.3 ± 3.0	667.9 ± 1.0	677.0 ± 1.0	64.6				
$Ti_{41}Zr_{25}Be_{28}Cu_6$	5	571.9 ± 3.0	640.3 ± 1.0	652.1 ± 1.0	68.4	316.2 ± 21.4	161.6 ± 9.2	185.7 ± 5.0	15
	10	576.1 ± 3.0	653.6 ± 1.0	663.4 ± 1.0	77.5				
	20	583.3 ± 3.0	671.0 ± 1.0	677.5 ± 1.0	87.7				
	40	589.2 ± 3.0	682.9 ± 1.0	691.3 ± 1.0	93.7				
$Ti_{41}Zr_{25}Be_{28}Ni_6$	5	584.5 ± 3.0	643.5 ± 1.0	657.7 ± 1.0	59.0	336.2 ± 21.0	134.2 ± 6.3	136.6 ± 6.5	15
	10	588.8 ± 3.0	658.1 ± 1.0	672.8 ± 1.0	69.3				
	20	595.9 ± 3.0	679.0 ± 1.0	694.3 ± 1.0	83.1				
	40	601.5 ± 3.0	695.5 ± 1.0	711.0 ± 1.0	94.0				
$Ti_{41}Zr_{25}Be_{28}V_6$	5	563.7 ± 3.0	610.3 ± 1.0	629.7 ± 1.0	46.6	395.7 ± 19.0	165.6 ± 12.9	211.9 ± 11.9	6
	10	568.0 ± 3.0	619.6 ± 1.0	639.3 ± 1.0	51.6				
	20	572.1 ± 3.0	632.5 ± 1.0	648.8 ± 1.0	60.4				
	40	577.7 ± 3.0	648.7 ± 1.0	662.3 ± 1.0	71.0				
$Ti_{41}Zr_{25}Be_{28}Cr_6$	5	581.2 ± 3.0	649.1 ± 1.0	660.1 ± 1.0	67.9	251.7 ± 19.1	168.7 ± 4.7	200.0 ± 6.2	8
	10	588.7 ± 3.0	663.9 ± 1.0	671.2 ± 1.0	75.2				
	20	595.3 ± 3.0	676.7 ± 1.0	683.5 ± 1.0	81.4				
	40	605.5 ± 3.0	692.8 ± 1.0	697.8 ± 1.0	87.3				

liquid region of Cu–Zr [29] and Cu–Zr–Al [30] alloys but decreases the activation energy of crystallization, which is attributed to a microstructural heterogeneity induced by Ag addition. In this sense, the addition of alloying elements may also induce inhomogeneity in Ti–Zr–Be alloy.

In order to find out the precipitation phases corresponding to different crystallization stages, samples were heated to the extrapolated end temperatures of different crystallization peaks, respectively, at a heating rate of 20 K min^{-1}, and cooled to room temperature. Figures 4 and S2 illustrate the crystallization behaviors of these eight BMGs. The corresponding crystalline phases of different alloys have been summarized in Table 2. For $Ti_{41}Zr_{25}Be_{34}$, $Ti_{41}Zr_{25}Be_{28}Al_6$, $Ti_{41}Zr_{25}Be_{28}Ag_6$, and $Ti_{41}Zr_{25}Be_{28}Cu_6$ alloys, the primary phase is indexed as α-Ti_2Zr. After complete crystallization beyond the highest crystallization peak temperature, more crystallization products such as Be_2Zr and α-Ti (α-TiZr for $Ti_{41}Zr_{25}Be_{28}Ag_6$ alloy) can be detected. For $Ti_{41}Zr_{25}Be_{28}Ni_6$ alloys, the first and second crystallization events are associated with the precipitation of α-Ti_2Zr and Be_2Zr phases, while α-Ti is detected after the third exothermic event. However, for $Ti_{41}Zr_{25}Be_{28}Fe_6$, $Ti_{41}Zr_{25}Be_{28}V_6$, and $Ti_{41}Zr_{25}Be_{28}Cr_6$ alloys, the

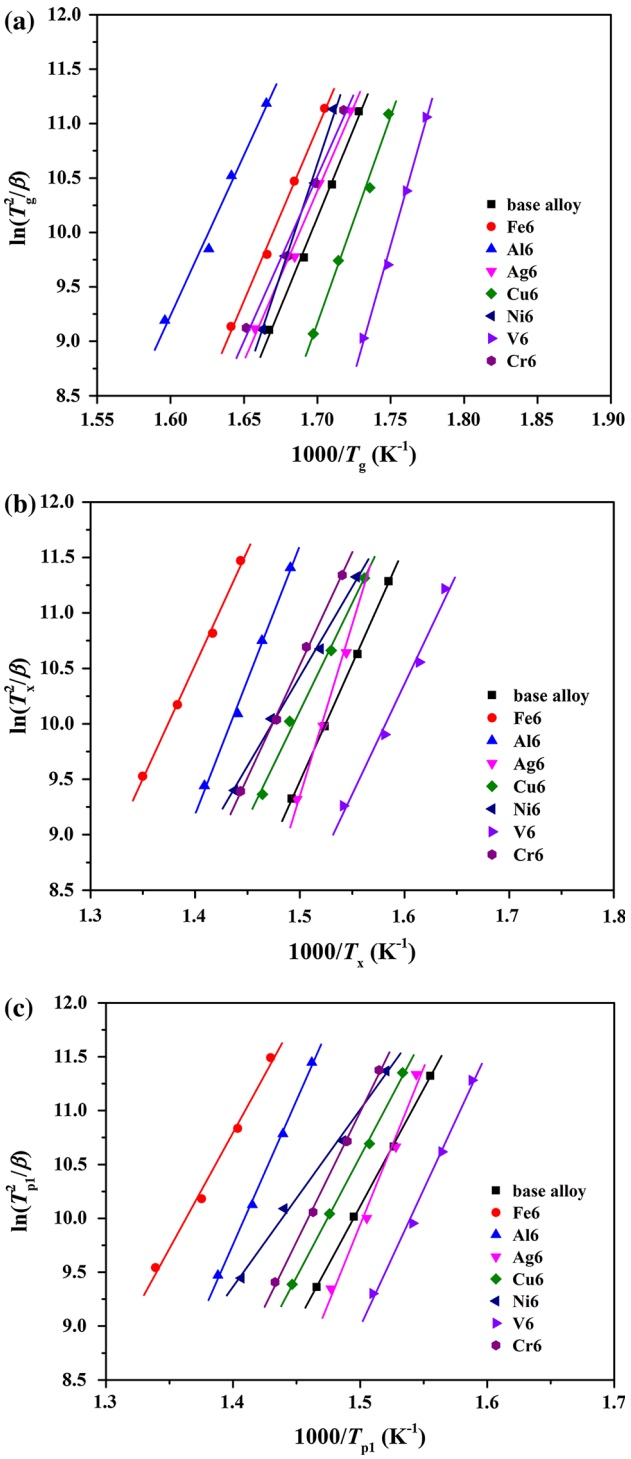

Figure 3 The activation energies corresponding to **a** T_g; **b** T_x; and **c** T_{p1} of $Ti_{41}Zr_{25}Be_{34}$ and $Ti_{41}Zr_{25}Be_{28}M_6$ (M = Fe, Al, Ag, Cu, Ni, V, and Cr) bulk metallic glasses generalized by Kissinger's method.

primary phase is no longer α-Ti_2Zr but β-Ti. This is because that Fe, V, and Cr are all typical beta-stabilizing elements which can lower the alpha-to-beta transition temperature. After the second crystallization event, instead of the Be_2Zr and α-Ti phases which are the crystalline phases for $Ti_{41}Zr_{25}Be_{28}V_6$ and $Ti_{41}Zr_{25}Be_{28}Cr_6$ samples, BeTi and α-Ti_2Zr phases are detected in $Ti_{41}Zr_{25}Be_{28}Fe_6$ sample. According to Zhang's research [14], for Ti–Zr–Be alloy system, the ternary eutectic consisting of two solution phases and one intermetallics exhibits lower GFA than that of the one solid solution and two intermetallics. So it is reasonable that $Ti_{41}Zr_{25}Be_{28}Fe_6$ alloy exhibits better GFA compared with $Ti_{41}Zr_{25}Be_{28}V_6$ and $Ti_{41}Zr_{25}Be_{28}Cr_6$ alloys. The above results indicate that the crystallization products especially the primary phase of Ti–Zr–Be ternary alloy can be selected according to demand by adding different alloying elements, and this is meaningful for preparing bulk metallic glass composite with good mechanical properties.

In order to further understand the crystallization kinetics of $Ti_{41}Zr_{25}Be_{34}$ and $Ti_{41}Zr_{25}Be_{28}M_6$ (M = Fe, Al, Ag, Cu, Ni, V or Cr) glassy alloys, the isothermal kinetics of the samples was characterized by annealing the samples at T_x-20 K and T_x-30 K (T_x here is measured at a heating rate of 20 K min^{-1}). The isothermal DSC curves of $Ti_{41}Zr_{25}Be_{34}$ alloy are shown in Fig. 5. The isothermal DSC curves of the other seven alloys are shown in Fig. S3 for reasons of simplicity. All DSC curves show a single exothermic peak after certain incubation time. With the increase of annealing time, it can be found that for all the Ti-based alloys, the incubation time decreases and the crystallization process becomes fast, which is in good agreement with previous reports [31–33]. It is also notable that $Ti_{41}Zr_{25}Be_{28}Fe_6$ alloy has a backward-shifted crystallization shape which means the crystallization rate is relatively low in the initial stage, while the other seven alloys have a forward-shifted bell shape. Based on the assumption that the fraction area of the crystallization peak is proportional to the crystallized volume fraction, the relationship between the crystallization volume fraction and annealing time during isothermal process can be obtained and the plots are shown in Fig. 6. All the curves display a typical sigmoidal trend. Except $Ti_{41}Zr_{25}Be_{28}Fe_6$ BMG, the alloys with higher GFA (e.g., $Ti_{41}Zr_{25}Be_{28}Ni_6$, $Ti_{41}Zr_{25}Be_{28}Cu_6$, and $Ti_{41}Zr_{25}Be_{28}Ag_6$ alloys) exhibits relatively long incubation time and broader crystallization peak, indicating their retarded crystallization process.

Details of the crystallization mechanism of $Ti_{41}Zr_{25}Be_{34}$ and $Ti_{41}Zr_{25}Be_{28}M_6$ (M = Fe, Al, Ag, Cu, Ni,

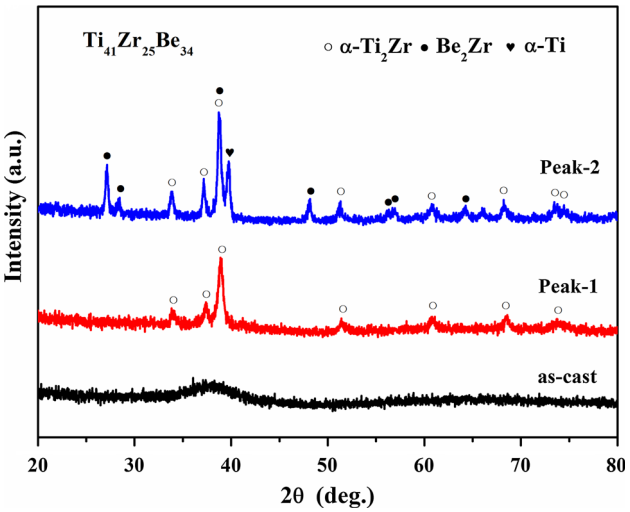

Figure 4 XRD patterns of $Ti_{41}Zr_{25}Be_{34}$ samples in the as-cast and annealed states.

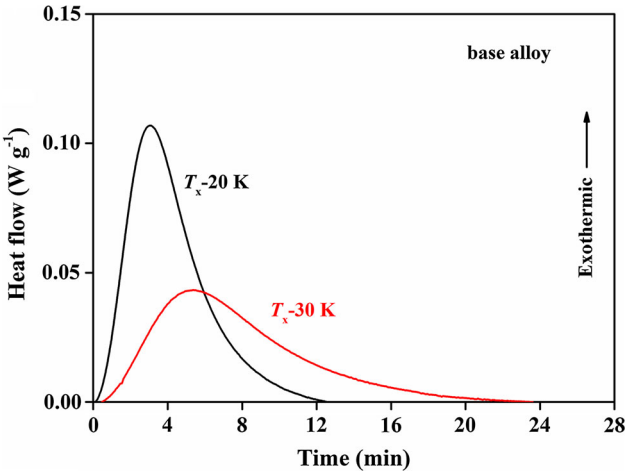

Figure 5 Isothermal DSC curves of $Ti_{41}Zr_{25}Be_{34}$ glassy alloy at T_x-20 K and T_x-30 K (T_x here is measured at a heating rate of 20 K min^{-1}).

V, or Cr) during isothermal annealing at T_x-30 K can be analyzed the Johnson–Mehl–Avrami (JMA) equation [34]:

$$\ln[-\ln(1-x)] = \ln k + n\ln(t-\tau), \quad (2)$$

where x is the crystallization volume fraction, t is the annealing time, n is the Avrami exponent which reflects the crystallization mechanisms of nucleation and growth, τ is the incubation time for crystallization, and k is a reaction rate constant. Figure 7 shows the JMA plots. As the incubation time of these Ti-based alloy is relatively short, only the data for $0.1 < x < 0.9$ are plotted in order to minimize the experimental error inherent in the early and late stages of the experiments. Although the corresponding JMA plots of the rest alloys are nearly straight lines, the JMA plot of $Ti_{41}Zr_{25}Be_{28}Fe_6$ alloy does not have a single slope, indicating the crystallization process of $Ti_{41}Zr_{25}Be_{28}Fe_6$ alloy is more complex than the other seven alloys. The average Avrami exponent n of $Ti_{41}Zr_{25}Be_{34}$, $Ti_{41}Zr_{25}Be_{28}Al_6$, $Ti_{41}Zr_{25}Be_{28}Ag_6$, $Ti_{41}Zr_{25}Be_{28}Cu_6$, $Ti_{41}Zr_{25}Be_{28}Ni_6$, $Ti_{41}Zr_{25}Be_{28}V_6$, and $Ti_{41}Zr_{25}Be_{28}Cr_6$ alloys are 1.97, 2.07, 2.20, 2.32, 2.32, 1.82, and 2.25, respectively.

As the crystallization mechanism of $Ti_{41}Zr_{25}Be_{28}Fe_6$ alloy changes dramatically during the process, the local Avrami exponent $n(x)$ is introduced and defined as [35]

$$n(x) = \frac{\partial \ln[-\ln(1-x)]}{\partial \ln(t-\tau)}. \quad (3)$$

The variation of the local Avrami exponent of $Ti_{41}Zr_{25}Be_{34}$ and $Ti_{41}Zr_{25}Be_{28}M_6$ (M = Fe, Al, Ag, Cu, Ni, V or Cr) alloys at T_x-30 K is shown in Fig. 8. In the case of $Ti_{41}Zr_{25}Be_{34}$ and $Ti_{41}Zr_{25}Be_{28}M_6$ (M = Al, Ag, Cu, Ni, V or Cr) alloys, the values of Avrami exponent at the early stage of the crystallization ($x = 0.1$) are 2.45, 2.58, 2.55, 2.68, 2.62, 2.29, and 2.73, respectively. With increasing crystallized volume fraction x, the n values of these seven alloys decrease to about 1.60 in the final

Table 2 Crystalline phases detected in the annealed $Ti_{41}Zr_{25}Be_{34}$ and $Ti_{41}Zr_{25}Be_{28}M_6$ (M = Fe, Al, Ag, Cu, Ni, V, and Cr) samples

Alloys	Peak-1	Peak-2
$Ti_{41}Zr_{25}Be_{34}$	α-Ti_2Zr	α-Ti_2Zr + Be_2Zr + α-Ti
$Ti_{41}Zr_{25}Be_{28}Fe_6$	β-Ti	β-Ti + BeTi + α-Ti_2Zr
$Ti_{41}Zr_{25}Be_{28}Al_6$	α-Ti_2Zr	α-Ti_2Zr + Be_2Zr + α-Ti
$Ti_{41}Zr_{25}Be_{28}Ag_6$	α-Ti_2Zr	α-Ti_2Zr + Be_2Zr + α-TiZr
$Ti_{41}Zr_{25}Be_{28}Cu_6$	α-Ti_2Zr	α-Ti_2Zr + Be_2Zr + α-Ti + unknown phase
$Ti_{41}Zr_{25}Be_{28}Ni_6$	α-Ti_2Zr + Be_2Zr	α-Ti_2Zr + Be_2Zr + α-Ti + unknown phase
$Ti_{41}Zr_{25}Be_{28}V_6$	β-Ti	β-Ti + Be_2Zr + α-Ti
$Ti_{41}Zr_{25}Be_{28}Cr_6$	β-Ti	β-Ti + Be_2Zr + α-Ti

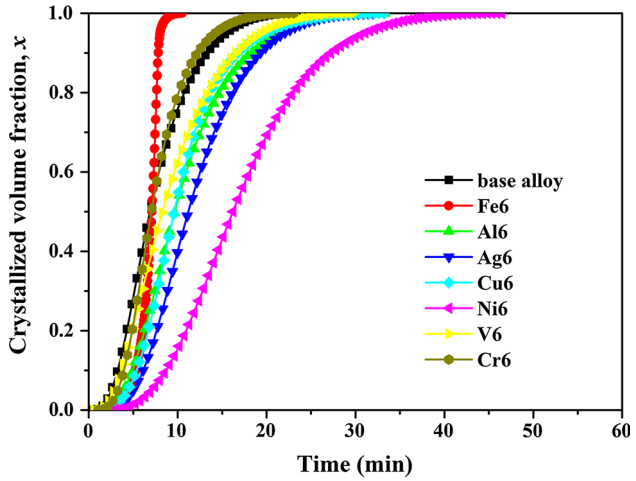

Figure 6 Plots of crystallized volume fraction versus annealing time of $Ti_{41}Zr_{25}Be_{34}$ and $Ti_{41}Zr_{25}Be_{28}M_6$ (M = Fe, Al, Ag, Cu, Ni, V, and Cr) glassy alloys.

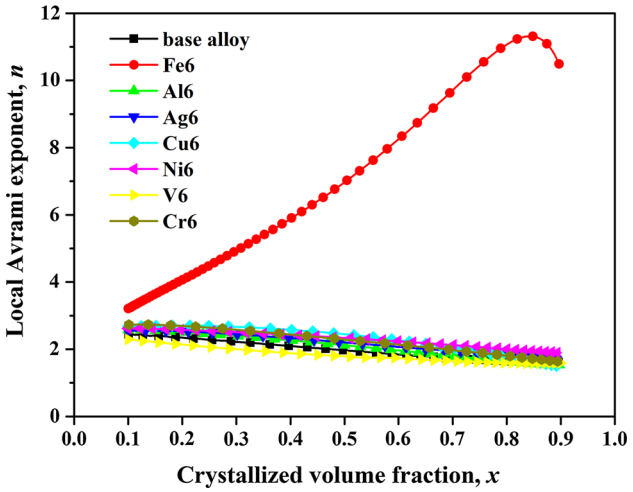

Figure 8 Local Avrami exponents $n(x)$ of $Ti_{41}Zr_{25}Be_{34}$ and $Ti_{41}Zr_{25}Be_{28}M_6$ (M = Fe, Al, Ag, Cu, Ni, V, and Cr) glassy alloy as a function of the crystallized volume fraction.

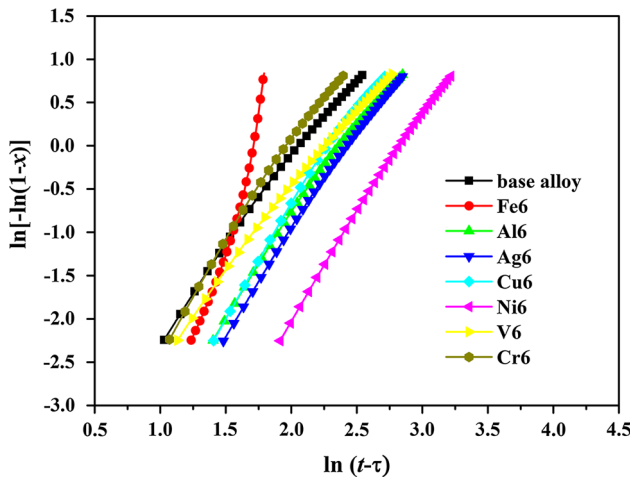

Figure 7 JMA plots of $Ti_{41}Zr_{25}Be_{34}$ and $Ti_{41}Zr_{25}Be_{28}M_6$ (M = Fe, Al, Ag, Cu, Ni, V, and Cr) glassy alloys.

stage ($x = 0.9$). On the other hand, the local Avrami exponent of $Ti_{41}Zr_{25}Be_{28}Fe_6$ alloy shows strong dependence on x with an average value of 5.26, which is much larger than those of $Ti_{41}Zr_{25}Be_{34}$ and $Ti_{41}Zr_{25}Be_{28}M_6$ (M = Al, Ag, Cu, Ni, V, or Cr) alloys.

The Avrami exponent n can be interpreted as [36]

$$n = a + bc, \tag{4}$$

where a is a parameter related with the nucleation rate ($a = 0$ for a zero nucleation rate, $0 < a < 1$ for a decreasing nucleation rate with time, $a = 1$ for a constant nucleation rate and $a > 1$ for an increasing nucleation rate). b is a parameter showing the dimension of the growth ($b = 1$, 2, and 3 for one-, two-, and three-dimensional growth, respectively). c is a parameter showing the type of growth ($c = 1$ for interface-controlled growth and $c = 0.5$ for diffusion-controlled growth). In this sense, the crystallization behavior of $Ti_{41}Zr_{25}Be_{34}$ and $Ti_{41}Zr_{25}Be_{28}M_6$ (M = Al, Ag, Cu, Ni, V, or Cr) alloys is mainly dominated by three-dimensional diffusion-controlled growth with a decreasing nucleation rate. $Ti_{41}Zr_{25}Be_{28}Fe_6$ alloy shows completely different crystallization behavior from the other alloys. The local Avrami exponent increases dramatically and then slightly decrease as the crystallized volume fraction x increases with a large value of 5.26, implying that the crystallization involves a transient nucleation process with an increasing nucleation rate [29]. Surface-induced abnormal grain growth with fractal dimensionality is also a possible reason [37].

Conclusions

The isochronal and isothermal crystallization behaviors of $Ti_{41}Zr_{25}Be_{34}$ and $Ti_{41}Zr_{25}Be_{28}M_6$ (M = Fe, Al, Ag, Cu, Ni, V, or Cr) glassy alloys have been studied using differential scanning calorimetry. It is indicated that the addition of Fe, Al, Cu, Ni, or Cr obviously enhances the thermal stability while the addition of Ag and V degrades the thermal stability slightly. No obvious relationship between the activation energy of

glass transition (or crystallization) and the glass-forming ability has been observed. Unlike Al, Ag, Cu, and Ni, the addition of Fe, V and Cr in $Ti_{41}Zr_{25}Be_{34}$ BMG leads to the change of primary crystalline phase from α-Ti_2Zr phase to β-Ti phase. The isothermal crystallization of $Ti_{41}Zr_{25}Be_{34}$ alloy is governed by three-dimensional diffusion-controlled growth with a decreasing nucleation rate. With the addition of Al, Ag, Cu, Ni, V, and Cr, there is no fundamental change in the overall nucleation and growth characteristics. However, for $Ti_{41}Zr_{25}Be_{28}Fe_6$ alloy, the local Avrami exponent shows strong dependence on crystallized volume fraction with a large average value of 5.26, implying a more complex crystallization process.

Acknowledgements

This work was supported by the National Natural Science Foundation of China (Grant No. 51271095).

Electronic supplementary material: The online version of this article (doi:10.1007/s10853-016-9835-5) contains supplementary material, which is available to authorized users.

References

[1] Yang H, Wang JQ, Li Y (2007) Glass formation and microstructure evolution in Al-Ni-RE (RE = La, Ce, Pr, Nd and misch metal) ternary systems. Philos Mag 87:4211–4228

[2] Sun BA, Pan MX, Zhao DQ, Wang WH, Xi XK, Sandor MT, Wu Y (2008) Aluminum-rich bulk metallic glasses. Scr Mater 59:1159–11621

[3] Zheng Q, Cheng S, Strader JH, Ma E, Xu J (2007) Critical size and strength of the best bulk metallic glass former in the Mg-Cu-Gd ternary system. Scr Mater 56:161–164

[4] Park ES, Lee JY, Kim DH (2005) Effect of Ag addition on the improvement of glass-forming ability and plasticity of Mg-Cu-Gd bulk metallic glass. J Mater Res 20:2379–2385

[5] Kim YC, Kim WT, Kim DH (2004) A develop of Ti-based bulk metallic glass. Mater Sci Eng A 375–377:127–135

[6] He G, Eckert J, Hagiwara M (2004) Glass-forming ability and crystallization behavior of Ti-CU-Ni-Sn-M (M = Zr, Mo, and Ta) metallic glasses. J Appl Phys 95:1816–1820

[7] Gong P, Wang X, Shao Y, Chen N, Liu X, Yao KF (2013) A Ti-Zr-Be-Fe-Cu bulk metallic glass with superior glass-forming ability and high specific strength. Intermetallics 43:177–181

[8] Jiang JZ, Hofmann D, Jarvis DJ, Fecht HJ (2014) Low-density high strength bulk metallic glasses and their composites: a review. Adv Eng Mater 17:761–780

[9] Wang YL, Xu J (2008) Ti(Zr)-Cu-Ni bulk metallic glasses with optimal glass-forming ability and their compressive properties. Metall Mater Trans A 39:2990–2997

[10] Xie KF, Yao KF, Huang TY (2010) A Ti-based bulk glassy alloy with high strength and good glass-forming ability. Intermetallics 18:1837–1841

[11] Guo FQ, Wang HJ, Poon SJ, Shiflet GJ (2005) Ductile titanium-based glassy alloy ingots. Appl Phys Lett 86:091907

[12] Zhu SL, Wang XM, Inoue A (2008) Glass-forming ability and mechanical properties of Ti-based bulk glassy alloys with large diameters of up to 1cm. Intermetallics 16:1031–1035

[13] Huang YJ, Shen J, Sun JF, Yu XB (2007) A new Ti-Zr-Hf-Cu-Ni-Si-Sn bulk amorphous alloy with high glass-forming ability. J Alloys Compd 427:171–175

[14] Zhang Y, Zhang WG, Lin JP, Hao GJ, Chen GL, Liaw PK (2010) Glass-forming ability and competitive crystalline phases for lightweight Ti-Be-based alloys. Metall Mater Trans A 41:1670–1676

[15] Duan G, Wiest A, Lind ML, Kahl A, Johnson WL (2008) Lightweight Ti-based bulk metallic glasses excluding late transition metals. Scr Mater 58:465–468

[16] Li YH, Zhang W, Dong C, Qiang JB, Makino A, Inoue A (2010) Formation and mechanical properties of Zr-Ni-Al glassy alloys with high glass-forming ability. Intermetallcs 18:1851–1855

[17] Ma H, Zheng Q, Xu J, Li Y, Ma E (2005) Doubling the critical size for bulk metallic glass formation in the Mg-Cu-Y ternary system. J Mater Res 20:2252–2255

[18] Gong P, Yao KF, Shao Y (2012) Lightweight Ti-Zr-Be-Al bulk metallic glasses with improved glass-forming ability and compressive plasticity. J Non-Cryst Solids 358:2620–2625

[19] Gong P, Yao KF, Shao Y (2012) Effects of Fe addition on glass-forming ability and mechanical properties of Ti-Zr-Be bulk metallic glass. J Alloys Compd 536:26–29

[20] Zhao SF, Shao Y, Gong P, Yao KF (2014) A centimeter-sized quaternary Ti-Zr-Be-Ag bulk metallic glass. Adv Mater Sci Eng 2014:192187

[21] Zhao SF, Chen N, Gong P, Yao KF (2015) New centimeter-sized quaternary Ti-Zr-Be-Cu bulk metallic glasses with large glass-forming ability. J Alloy Compd 647:533–538

[22] Zhao SF, Gong P, Li JF, Chen N, Yao KF (2015) Quaternary Ti-Zr-Be-Ni bulk metallic glasses with large glass-forming ability. Mater Des 85:564–573

[23] Patel A, Pratap A (2012) Kinetics of crystallization of $Zr_{52}Cu_{18}Ni_{14}Al_{10}Ti_6$ metallic glass. J Therm Anal Calorim 107:159–165

[24] Wang T, Yang XH, Li Q (2014) Effect of Cu and Nb additions on crystallization kinetics of Fe80P13C7 bulk metallic glasses. Thermochim Acta 579:9–14

[25] Gong P, Yao KF, Ding HY (2015) Crystallization kinetics of TiZrHfCuNiBe high entropy bulk metallic glass. Mater Lett 156:146–149

[26] Lu ZP, Liu CT (2002) A new glass-forming ability criterion for bulk metallic glasses. Acta Mater 50:3501–3512

[27] Kissinger HE (1957) Reaction kinetics in differential thermal analysis. Anal Chem 29:1702–1706

[28] Wang HR, Gao YL, Min GH, Hui XD, Ye YF (2003) Primary crystallization in rapidly solidified $Zr_{70}Cu_{20}Ni_{10}$ alloy from a supercooled liquid region. Phys Lett A 314:81–87

[29] Song KK, Gargarella P, Pauly S, Ma GZ, Kühn U, Eckert J (2012) Correlation between glass-forming ability, thermal stability, and crystallization kinetics of Cu-Zr-Ag metallic glass. J Appl Phys 112:063505

[30] Sung DS, Kwon OJ, Fleury E, Kim KB, Lee JC, Kim DH, Kim YC (2004) Enhancement of the glass forming ability of Cu-Zr-Al alloys by Ag addition. Met Mater Int 10:575–579

[31] Qiao JC, Pelletier JM (2011) Crystallization kinetics in $Cu_{46}Zr_{45}Al_7Y_2$ bulk metallic glass by differential scanning calorimetry. J Non-Cryst Solids 357:2590–2594

[32] Jung HY, Stoica M, Yi SH, Kim DH, Eckert J (2014) Crystallization kinetics of $Fe_{76.5-x}C_{6.0}Si_{3.3}P_{8.7}Cu_x$ ($x = 0$, 0.5, and 1 at. pct) bulk amorphous alloy. Metall Mater Trans A 46:2415–2421

[33] Hua NB, Chen WZ, Liu XL, Yue F (2014) Isochronal and isothermal crystallization kinetics of Zr-Al-Fe glassy alloys: effects of high-Zr content. J Non-Cryst Solids 388:10–16

[34] Avrami M (1941) Granulation, phase change, and microstructure kinetics of phase change. III. J Chem Phys 9:177–184

[35] Calka A, Radlinski AP (1988) Decoupled bulk and surface crystallization in $Pd_{85}Si_{15}$ glassy metallic alloys: description of isothermal crystallization by a local value of the Avrami exponent. J Mater Res 3:59–66

[36] Ranganathan S, Heimendahl MV (1981) The three activation energies with isothermal transformations: applications to metallic glasses. J Mater Res 16:2401–2404

[37] Pratap A, Raval KG, Gupta A, Kulkarni SK (2000) Nucleation and growth of a multicomponent metallic glass. Bull Mater Sci 23:185–188